Journal of Radiation Research, 2015, 56, 372–381
doi: 10.1093/jrr/rru106 Advance Access Publication 23 January 2015

Development of a wavelength-separated type scintillator with optical fiber (SOF) dosimeter to compensate for the Cerenkov radiation effect

Masayori ISHIKAWA[1,*], Naomi NAGASE[2], Taeko MATSUURA[3], Junichi HIRATSUKA[2], Ryusuke SUZUKI[3], Naoki MIYAMOTO[1], Kenneth Lee SUTHERLAND[1], Katsuhisa FUJITA[4] and Hiroki SHIRATO[5]

[1]Department of Medical Physics and Engineering, Graduate School of Medicine, Hokkaido University, N-15 W-7 Kita-ku, Sapporo Hokkaido, 060-8638, Japan
[2]Department of Radiology, Kawasaki Medical School Hospital, 577 Matsushima, Kurashiki Okayama, 701-0192, Japan
[3]Department of Medical Physics, Hokkaido University Hospital, N-14 W-5 Kita-ku, Sapporo Hokkaido, 060-8648, Japan
[4]Department of Radiology, Hokkaido University Hospital, N-14 W-5 Kita-ku, Sapporo Hokkaido, 060-8648, Japan
[5]Department of Radiology, Graduate School of Medicine, Hokkaido University, N-15 W-7 Kita-ku, Sapporo Hokkaido, 060-8638, Japan
*Corresponding author. Department of Medical Physics and Engineering, Graduate School of Medicine, Hokkaido University, N-15 W-7 Kita-ku, Sapporo Hokkaido, 060-8638, Japan. Tel: +81-11-706-7638; Fax: +81-11-706-7639; Email: masayori@med.hokudai.ac.jp

(Received 24 June 2014; revised 2 September 2014; accepted 7 October 2014)

The scintillator with optical fiber (SOF) dosimeter consists of a miniature scintillator mounted on the tip of an optical fiber. The scintillator of the current SOF dosimeter is a 1-mm diameter hemisphere. For a scintillation dosimeter coupled with an optical fiber, measurement accuracy is influenced by signals due to Cerenkov radiation in the optical fiber. We have implemented a spectral filtering technique for compensating for the Cerenkov radiation effect specifically for our plastic scintillator-based dosimeter, using a wavelength-separated counting method. A dichroic mirror was used for separating input light signals. Individual signal counting was performed for high- and low-wavelength light signals. To confirm the accuracy, measurements with various amounts of Cerenkov radiation were performed by changing the incident direction while keeping the Ir-192 source-to-dosimeter distance constant, resulting in a fluctuation of <5%. Optical fiber bending was also addressed; no bending effect was observed for our wavelength-separated SOF dosimeter.

Keywords: Cerenkov light removal; plastic scintillator dosimetry; pulse counting mode; SOF dosimeter; Ir-192 brachytherapy

INTRODUCTION

Recently, as CT-based 3D radiation treatment-planning systems (RTPs) for brachytherapy have become more accessible, the importance of sparing organs at risk (OARs) from tolerant dose has been increasing for high-precision radiation therapy. Although *in vivo* dosimetry is preferable for verifying the delivered dose for tumors and OARs, some tumors and OARs are located deep inside the patient body, making direct measurement difficult. The small Si photo-diode detector and the MOSFET detector appear to be suitable *in vivo* dosimeters [1, 2]. However, the material composition of these semiconductor detectors is not tissue-equivalent. Moreover, metal wires and cables are necessary for supplying electric power and transmitting signals from these detectors, which inevitably affect the measured dose for therapeutic radiation.

The use of a small plastic scintillation dosimeter coupled to an optical fiber was proposed and developed by Beddar *et al.*, Arnfield *et al.*, Fluhs *et al.*, Geso *et al.*, Lambert *et al.* and Sliski *et al.* [3–9]. We have also developed a novel plastic scintillator-based dosimeter with pulse-counting mode [10]. While dosimeters using materials other than plastic coupled to an optical fiber have long been available [11, 12], a plastic scintillator dosimeter is practically more suitable for photon dosimetry because the amount of light emissions from the scintillator is proportional to the absorbed

dose. The composition of a plastic scintillator is similar to human tissue; therefore, it has little influence on the measured dose. The mean mass–energy absorption coefficient of the plastic scintillator is relatively close to that of water above 200 keV, as is the mass collision stopping power and the mass angular scattering power. Furthermore, light signals from the scintillator to the counting device can be transmitted through a plastic optical fiber, which maintains the tissue-equivalent composition of the entire detector.

On the other hand, high-energy radiation produces Cerenkov radiation in materials [13]. This Cerenkov radiation is well known as an additional signal for plastic scintillation dosimeters, especially coupled with an optical fiber. Beddar *et al.* first described the Cerenkov Effect in 1992 [3], employing a simple subtraction method to remove the Cerenkov radiation effect and quantifying the stem effect [6, 14]. Several research projects have been undertaken seeking to minimize the Cerenkov radiation effect. Beddar *et al.* and Clift *et al.* tried to compensate for the effect by subtracting two fibers, one with and one without a scintillator [15–17]. A spectral filtering technique, or a gating method, has also been investigated [18, 19]. Archambault *et al.* and Guillot *et al.* tried to separate signals between scintillation and Cerenkov light using a dichroic filter [20, 21]. Lambert *et al.* developed a Cerenkov-free dosimetry system by using an air-core light guide [22].

In this paper, we implement a spectral filtering technique for compensating for the Cerenkov radiation effect specifically for our plastic scintillator-based dosimeter by using a wavelength-separated counting method and report the results of our investigation for high-dose-rate ^{192}Ir irradiation.

MATERIALS AND METHODS

Description of the scintillation dosimeter

Figure 1 shows the components of our scintillation dosimetry system reported previously [10]. In the succeeding discussion, we refer to this dosimeter as the scintillator with optical fiber (SOF) dosimeter. The scintillator material we used was BC490 plastic manufactured by Saint-Gobain Ltd. BC490 is partially polymerized and hardened by a catalyst, which makes it possible to be tightly attached to the tip of a plastic optical fiber (MH4001 manufactured by Mitsubishi Rayon Co. Ltd, reflective index of 1.49, 1-mm diameter optical fiber with 2.2-mm diameter polyethylene shielding). The plastic scintillator is shaped into a hemisphere with a diameter of 1 mm and an active volume of 0.26 mm^3. Hemispherical shape is advantageous for better angular response to the incident radiation. The photon signals are relayed through the optical fiber onto the Photon Counting Head (Hamamatsu H7155), then converted into 30-ns-width TTL pulses. The counting unit is made up of a photomultiplier tube, a charge pre-amplifier and a discriminator. The pulse counts are transmitted to a personal computer via a universal serial bus (USB) connection. The measurable

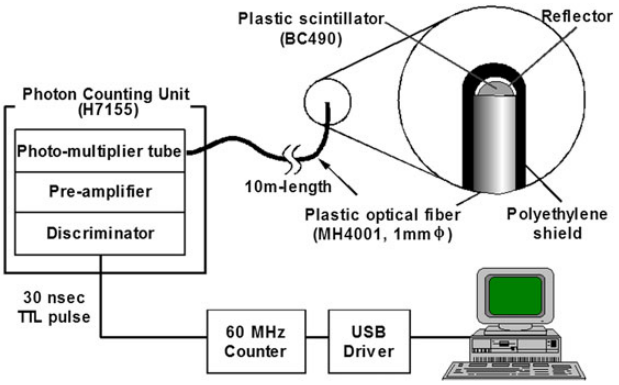

Fig. 1. Schematic diagram of SOF dosimeter system. The SOF dosimeter made up of a small plastic scintillator, a plastic optical fiber, a photon counting unit and data acquisition system connected to a personal computer via USB.

range of the SOF dosimeter, which is from 11.4 cGy min^{-1} to 1.15×10^4 cGy min^{-1}, covers a range of almost 10^3 cGy min^{-1} without switching measurement range [10].

The absorbed dose in the water D_W can be described as

$$D_W = \alpha(C_{Sc} + \beta\Delta t), \tag{1}$$

where C_{Sc} is the pulse count corresponding to the number of energy deposition events in the scintillator from the radiation with energy greater than $E_{0,}$ which was denoted by the symbol C_{total} in our previous paper [10], Δt is the duration of the measurement, α and β are the correction coefficients for converting count to dose, which can be expressed using calibration coefficients a [counts s^{-1} J^{-1}] and b [J^{-1}] by

$$\alpha = \frac{1(\mu_{en}/\rho)_W}{bm(\mu_{en}/\rho)_{Sc}},\ \beta = \frac{a}{b}\{1 - \exp(-bE_0)\}, \tag{2}$$

where, m is the mass of the scintillator, $(\mu_{en}/\rho)_w$ and $(\mu_{en}/\rho)_{sc}$ are the mass energy absorption coefficient for water and scintillator, respectively, and E_0 is the threshold energy for pulse counting. The parameter a is nuclei dependent, whereas parameter b is almost energy independent. C_{Sc} can also be expressed as

$$C_{sc} = a\Delta t \int_{E_0}^{\infty} \exp(-bE)dE = \frac{a\Delta t}{b}\exp(-bE_0). \tag{3}$$

By using Eq. (3), $\beta\Delta t$ can be expressed as

$$\beta\Delta t = \frac{C_{Sc}}{\exp(-bE_0)} - C_{Sc}. \tag{4}$$

Finally, the absorbed dose in the water D_w is simplified as

$$D_W = \alpha' C_{Sc}, \qquad \alpha' = \frac{(\mu_{en}/\rho)_W}{(\mu_{en}/\rho)_{Sc}} \frac{1}{bm\exp(-bE_0)}. \tag{5}$$

Signal separation by a dichroic mirror

Figure 2 shows photographs of the wavelength-separated type SOF (WS-SOF) dosimeter used in this study. A dichroic mirror was placed facing at 45° from the optical fiber axis. As shown in Fig. 2, signals reflected by the dichroic mirror were defined as Ch1, while signals transparent through the dichroic mirror were defined as Ch2. Ch1 and Ch2 consist of the sum of scintillation signals C_{Sc} and Cerenkov signals C_{Cere} with some scale factors. A pair of the H7155 photon counting heads detect separated light signals. The scintillation spectrum of the BC490 plastic scintillator and Cerenkov radiation generated by ^{192}Ir is shown in Fig. 3. The plastic scintillator has a peak wavelength at 420 nm, whereas the spectrum of Cerenkov radiation varies over a wide range in the visible spectrum. Since these two spectra are quite different, we tried to distinguish contributions from them separately by using a dichroic mirror, setting an adequate threshold wavelength (λ_{th}).

The spectrum of the BC490 plastic scintillator is distributed relatively lower compared with that of Cerenkov radiation. The threshold wavelength was set at 465 nm to preserve as much signal as possible with adequate removal of the Cerenkov radiation effect. The dichroic mirror was ordered with a 465-nm threshold wavelength at 45° respect to the incident light path. As shown in Fig. 3, we defined I_{L_BC490} as the sum of intensities of BC490, which were lower than the threshold, I_{L_Cere}, the sum of intensities of Cerenkov radiation, which were lower than the threshold, I_{H_BC490}, the sum of intensities of BC490, which were higher than the threshold, and I_{H_Cere}, the sum of intensities of Cerenkov radiation, which were higher than threshold.

Assuming that scintillation signals are counted as C_{Sc} by the single photon-counting unit, signals divided by the dichroic mirror should have smaller pulse counts due to smaller pulse height with an adequate discriminator level for eliminating electronic noise. Count reduction factors due to separating signals by the dichroic mirror for the scintillation and Cerenkov radiation are defined a_{Sc} and a_{Cere}, respectively. To simplify the equations, efficiency ratios are defined as k_{Sc} and k_{Cere} due to the efficiency difference between the photomultiplier tubes for Ch1 and Ch2. Here, k_{Sc} and k_{Cere} not

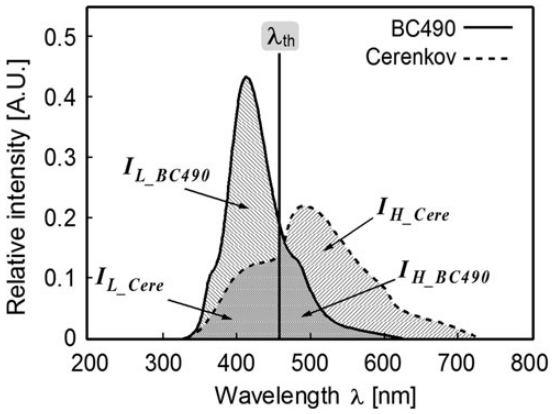

Fig. 3. Measured spectra of BC490 plastic scintillator and Cerenkov radiation. I_{L_BC490}, I_{L_Cere}, I_{H_BC490}, I_{H_Cere} represent sum of intensities of BC490 lower than threshold, sum of intensities of Cerenkov radiation lower than threshold, sum of intensities of BC490 higher than threshold, sum of intensities of Cerenkov radiation higher than threshold, respectively.

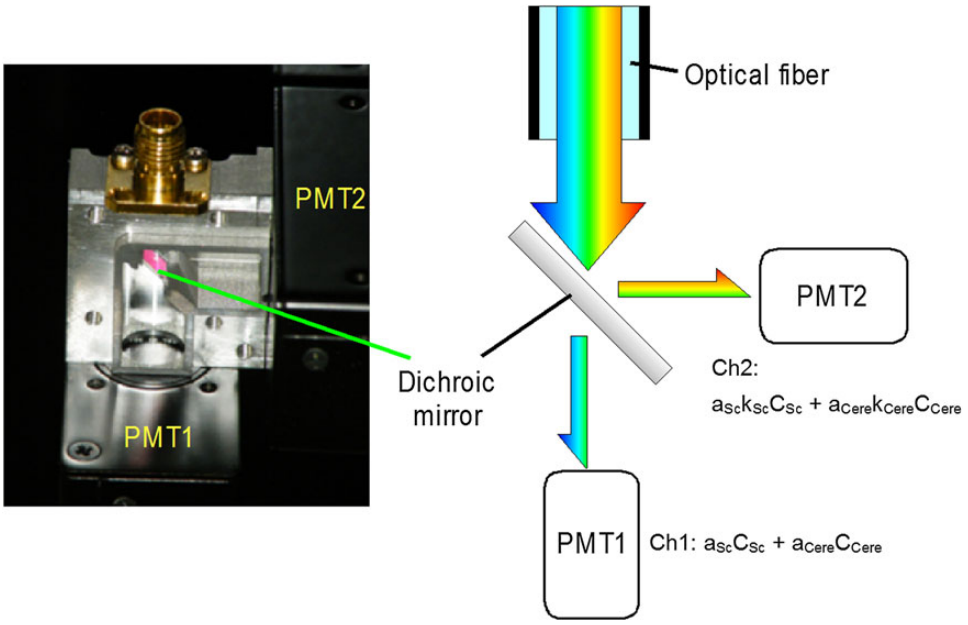

Fig. 2. Photographs of the wavelength-separated type SOF dosimeter. A dichroic mirror was placed just after the SMA connector to split the spectrum of light signals by threshold wavelength.

only include efficiency difference but also the reflection/transparent ratio due to the dichroic mirror.

$$\mathrm{Ch1} = \mathrm{a_{Sc}C_{sc}} + \mathrm{a_{Cere}C_{Cere}} \qquad (> \lambda_{th}) \tag{6}$$

$$\mathrm{Ch2} = \mathrm{a_{Sc}}k_{\mathrm{Sc}}\mathrm{C_{Sc}} + \mathrm{a_{Cere}}k_{\mathrm{Cere}}\mathrm{C_{Cere}} \qquad (< \lambda_{th}) \tag{7}$$

The basic concept is very similar to the spectral filter technique proposed by Fontbonne *et al.* [18]. From equations (6) and (7), C_{Sc} and C_{Cere} are deduced as follows:

$$\mathrm{a_{Sc}C_{sc}} = \frac{k_{\mathrm{Cere}}\mathrm{Ch1} - \mathrm{Ch2}}{k_{\mathrm{Cere}} - k_{\mathrm{Sc}}} \tag{8}$$

$$\mathrm{a_{Cere}C_{Cere}} = \frac{k_{\mathrm{Sc}}\mathrm{Ch1} - \mathrm{Ch2}}{k_{\mathrm{Sc}} - k_{\mathrm{Cere}}}. \tag{9}$$

Scintillation signals and Cerenkov signals can be estimated by the number of counts of Ch1 and Ch2 with correction coefficients k_{Sc} and k_{Cere}.

Experiments

Calibration for correction coefficient k_{Sc} and k_{Cere}

Generally, low-energy photons (e.g. under 100 keV) do not generate Cerenkov radiation in the plastic optical fiber. However, generation of a fluorescence from the optical fiber itself might be observed when irradiated with even low-energy photons (10 keV), and thus the optical fiber was shielded with 2-mm-thick lead sheet for this calibration process. A 10-kV X-ray source generated by ECLIPSE III (manufactured by AmpTek Co. Ltd, Ag target) was used to evaluate k_{Sc}. The influence of Cerenkov radiation can be ignored by using low-energy photons. Eqs. (6) and (7) can be simplified as follows:

$$\mathrm{Ch1_{low}} = \mathrm{a_{Sc}C_{sc}} \tag{10}$$

$$\mathrm{Ch2_{low}} = \mathrm{a_{Sc}}k_{\mathrm{Sc}}\mathrm{C_{Sc}} \tag{11}$$

Then k_{Sc} can be calculated by

$$k_{\mathrm{Sc}} = \frac{\mathrm{Ch2_{low}}}{\mathrm{Ch1_{low}}}. \tag{12}$$

Calibration for the coefficients of k_{Cere} was performed by two measurements for which the dose at the scintillator was the same but the amount of Cerenkov radiation was different. Assuming that the calibration geometry of A and B have the same gamma-ray intensity as the scintillators but have different Cerenkov intensities to the optical fiber, each channel count can be expressed as follows:

$$\begin{pmatrix} \mathrm{Ch1_A} & \mathrm{Ch1_B} \\ \mathrm{Ch2_A} & \mathrm{Ch2_B} \end{pmatrix} = \begin{pmatrix} 1 & 1 \\ k_{\mathrm{Sc}} & k_{\mathrm{Cere}} \end{pmatrix} \times \begin{pmatrix} \mathrm{a_{Sc}C_{Sc,A}} & \mathrm{a_{Sc}C_{Sc,B}} \\ \mathrm{a_{Cere}C_{Cere,A}} & \mathrm{a_{Cere}C_{Cere,B}} \end{pmatrix} \tag{13}$$

$$\mathrm{C_{Sc,A}} = \mathrm{C_{Sc,B}}. \tag{14}$$

From Eqs. (13) and (14), k_{Cere} can be deduced as

$$k_{\mathrm{Cere}} = \frac{\mathrm{Ch2_A} - \mathrm{Ch2_B}}{\mathrm{Ch1_A} - \mathrm{Ch1_B}}. \tag{15}$$

Similarly, the water equivalent dose can be expressed by the following equation:

$$\mathrm{D}_W = \alpha'\mathrm{C_{sc}} = \frac{\alpha'}{\mathrm{a_{Sc}}}\mathrm{a_{Sc}C_{sc}} = \frac{\alpha'}{\mathrm{a_{Sc}}}\frac{k_{\mathrm{Cere}}\mathrm{Ch1} - \mathrm{Ch2}}{k_{\mathrm{Cere}} - k_{\mathrm{Sc}}}. \tag{16}$$

In this study, microSelectron HDR (manufactured by Nucletron Co. Ltd) was used for the ^{192}Ir source. Source calibration details are shown in Table 1. For the probe calibration, the Afterloading calibration phantom (type 9193 manufactured by Nucletron Co. Ltd) was used. As shown in Fig. 4, the phantom is made of 20 cmϕ × 12 cm Polymethylmethacrylate (PMMA) with four holes with diameter of 2 cmϕ at 8 cm distance from the ^{192}Ir source position (phantom center). At the distance of 8 cm, the absorbed dose rate is adjusted to ~1 cGy/min when the 37 GBq ^{192}Ir source is used (type 9193 phantom user's manual) [23]. The water-equivalent dose is calculated as follows:

$$\begin{aligned} \dot{\mathrm{D}}_{\mathrm{w,zp}} &= (1 - g_{\mathrm{w}}) \cdot (\mu_{\mathrm{en}}/\rho)_{\mathrm{w}} \cdot (\mu_{\mathrm{en}}/\rho)_{\mathrm{a}} \cdot \frac{1}{\mathrm{k_r}} \cdot \frac{1}{\mathrm{k_{zp}}} \cdot (\dot{\mathrm{K}}_{\mathrm{a}})_{\mathrm{a}} \\ &= 0.2435 \cdot (\dot{\mathrm{K}}_{\mathrm{a}})_{\mathrm{a}} (\mathrm{cGY/min@8cm}). \end{aligned} \tag{17}$$

Here, $\dot{\mathrm{D}}_{\mathrm{w,zp}}$ is the reference absorbed dose rate to water in the cylindrical phantom at 8 cm distance from the source center, $(\dot{\mathrm{K}}_{\mathrm{a}})_{\mathrm{a}}$ is the air kerma rate in air at 100 cm distance, g_{w} is the relative Bremsstrahlung loss in water for ^{192}Ir, and $(\mu_{\mathrm{en}}/\rho)_{\mathrm{w}}$ and $(\mu_{\mathrm{en}}/\rho)_{\mathrm{a}}$ are the mass energy absorption coefficient for

Table 1. ^{192}Ir source calibration data

	Air kerma rate (mGy·h^{-1}@1m)	Absorbed dose rate at calibration point (cGy·min^{-1}@8cm)	
		Calculated	Measured
Calibrated at 31 Aug. 2012	43.81	7.334	
Experiment at 24 Nov. 2012	26.42	6.433	6.424 ± 0.007

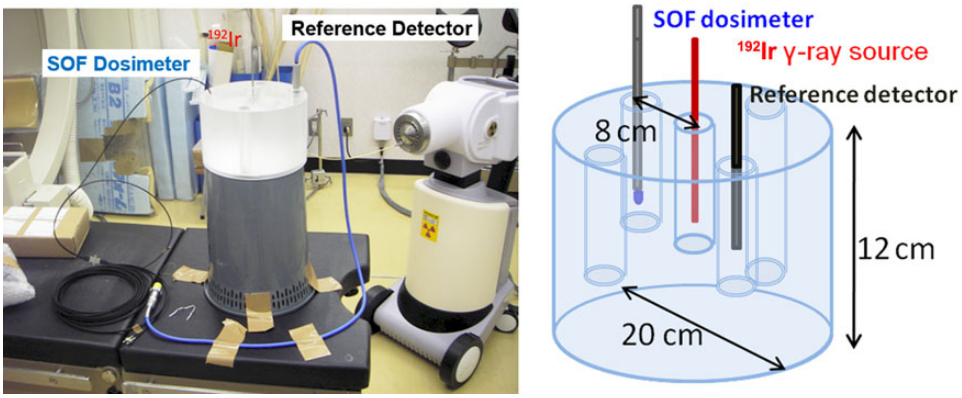

Fig. 4. Calibration geometry using Afterloading calibration phantom type 9193.

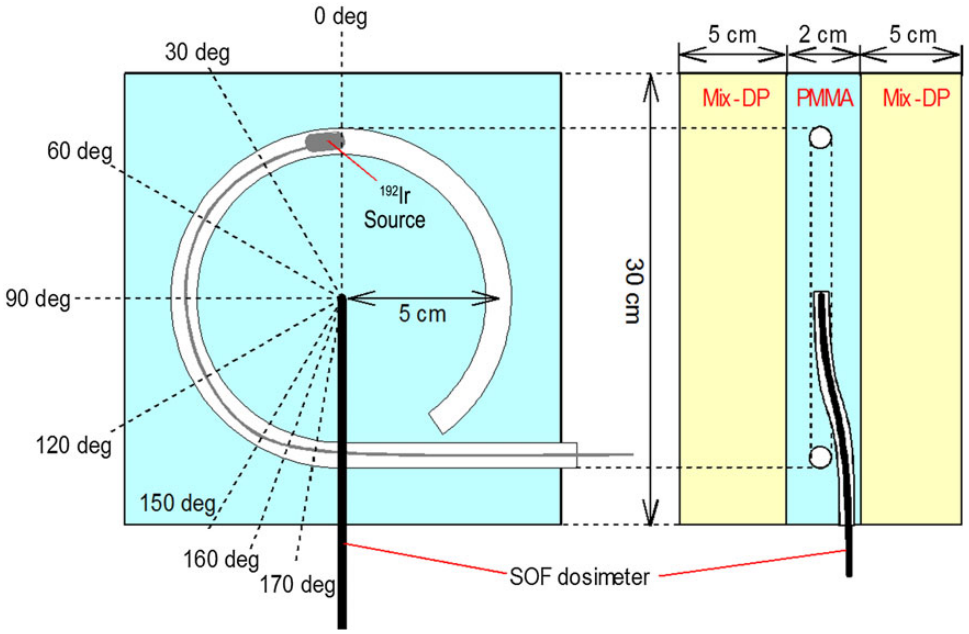

Fig. 5. Experiment geometry for assessment of the scintillation–Cerenkov signal separation.

water and air, respectively. k_r and k_{zp} are correction factors for the inverse square of the distance and geometry for the cylindrical phantom, respectively; here these values are defined as $k_r = (8/100)^2 = 0.0064$ and $k_{zp} = 1.187 \pm 0.012$. The absorbed dose rate at the calibration point was confirmed by measurement using a Farmer type ionization chamber (PTW30004). The difference between calculation and measurement was 0.13%.

Scintillation–Cerenkov signal separation

In this study, two probes with differing sensitivities were used. Probe #1 is a normal probe with an estimated volume of 0.234 mm^3, while probe #2 has a smaller scintillator with a volume of 0.106 mm^3 to enhance the Cerenkov radiation effect. In order to assess the accuracy of the scintillation–Cerenkov signal separation method, measurements were performed with the geometry shown in Fig. 5. A $30 \times 30 \times 2$ cm^3 PMMA phantom with a guide sleeve was placed at a 5-cm distance from the phantom center, which is the location of the SOF dosimeter probe. For gathering scattering gamma rays, 5-cm-thick Mix-DP phantoms were placed on both sides of the PMMA phantom as shown in Fig. 5. Zero degrees is defined toward the tip of the SOF dosimeter. Measurements were acquired at 0, 30, 60, 90, 120, 150, 160, 170 and 180°. The 180° position was the closest to the ^{192}Ir source; the distance was ~2 mm. Acquisition times for each measurement point were 20 s, repeated five times. Calibration measurements were acquired for 60 s, repeated 10 times.

Table 2. Correction coefficients k_{Sc}, k_{Cere} and conversion factors

Probe	k_{Sc}	k_{Cere}		α/a_{Sc} [cGy/counts]		Relative efficiency
		0 & 160 deg	0 & 180 deg	0 & 160 deg	0 & 180 deg	
#1	0.367 (0.46%)[a]	0.991 (1.31%)	0.994 (0.22%)	5.981×10^{-5} (3.76%)	5.998×10^{-5} (1.15%)	1
#2	0.340 (0.81%)	1.029 (1.11%)	1.027 (0.20%)	1.364×10^{-4} (2.70%)	1.365×10^{-4} (1.30%)	0.439

[a]Estimated uncertainties are indicated in parentheses. Uncertainty in the ^{192}Ir source is not included.

Comparison with MCNPX calculation

In order to justify the measurements obtained from WS-SOF dosimeter, a comparison with MCNPX 2.4 Monte Carlo code was performed. Measurement and calculation was performed in a $30 \times 30 \times 30$ cm^3 water phantom with a 5-mm-thickness PMMA wall. An ^{192}Ir source was fixed at the center of the phantom. The SOF dosimeter probe was scanned along an axis 1 cm away from the ^{192}Ir source. The scan range was −100 mm to +100 mm on the axis with 10-mm intervals. Additional measurements were performed within 10 mm with 1-mm intervals. The measurement at each position was performed four times with a 10-min acquisition time. The ^{192}Ir source strength at the experiment date was 26.42 mGy m^2 h^{-1}.

RESULTS

Calibration for correction coefficients k_{Sc} and k_{Cere}

Correction coefficients k_{Sc} and k_{Cere} are shown in Table 2. For k_{Cere} calibration, the ^{192}Ir source was placed at the 0° & 160° positions and the 0° & 180° positions in the same geometry of Fig. 5. Conversion factor α' cannot be deduced in our theory; however, α'/a_{Sc} can be estimated by comparing the value of $a_{Sc}C_{Sc}$ with the absolute dose measurement.

As mentioned in the Experiments section, the calibration process requires two different conditions which have different amount of Cerenkov radiation to the fiber with exactly same gamma-ray incidence from Ir-192 source. As shown in Fig. 5, the 0° and 180° positions are the minimum and maximum position influenced by Cerenkov radiation, respectively. On the contrary, a small Cerenkov radiation effect is expected at the 160° position. The 0° & 160° and 0° & 180° positions were selected for the calibration process in order to compare the calibration accuracy due to the amount of the Cerenkov radiation.

Experiment for scintillation–Cerenkov signal separation

Figure 6 shows the angular dependency for separated signals of scintillation and Cerenkov radiation as a function of incident angle for two probes for which calibrations were calibrated with 0° and 160° source position values. Figure 7 shows the angular dependency with 0° and 180° source position values. All values in Figs 6 and 7 were calculated by Eq. (6) and Eq. (7), normalized at the scintillation signal of 0° position. As shown in Fig. 6, the estimated scintillation signals for calibration with 0° & 160° positions were influenced by an increase of Cerenkov light. A more accurate calibration can be performed using 0° & 180° data, which contains sufficient Cerenkov signals. Relative estimation errors $\%\,\sigma_{Dw}$ for the relative absorbed dose %Dw in Figs 6 and 7 were deduced from error propagation formula as described below:

$$\%\sigma_{D_W} = \frac{k_{Cere}^2\sigma_{Ch1}^2 + \sigma_{Ch2}^2}{(k_{Cere} - k_{Sc})^2} + \frac{(Ch2 - k_{Cere}Ch1)}{(k_{Cere} - k_{Sc})^4}\sigma_{k_{Sc}}^2 + \frac{Ch1^2(Ch2 - k_{Cere}Ch1)^2}{(k_{Cere} - k_{Sc})^6}\sigma_{k_{Cere}}^2. \quad (18)$$

Here, σ_{Ch1} and σ_{Ch2} are measurement uncertainty for Ch1 and Ch2, and $\sigma_{k_{Sc}}$ and $\sigma_{k_{Cere}}$ are estimation uncertainty for parameters of k_{Sc} and k_{Cere}, respectively.

Comparison with MCNPX calculation

Figure 8a and 8b shows the results of the SOF measurement and the MCNPX 2.4 calculation. The values for the MCNPX calculation were normalized at the −50 mm position with the value of SOF probe #1. The maximum differences between the SOF measurement and the MCNPX calculation for probes #1 and #2 were 5.06% and 4.80%, respectively, whereas for the limited range within 10 mm, the maximum differences were 0.90% and 2.07%, respectively. Therriaut-Proulx *et al.* [23] performed a phantom study using a plastic scintillator detector (PSD) based on *in vivo* dosimetry for HDR ^{192}Ir brachytherapy. The measurement agreed within 6% compared with the calculation of a treatment-planning system. Our results are comparative with these results.

On the other hand, if the compensation for Cerenkov radiation is not performed, the maximum differences between the SOF measurement and the MCNPX calculation for probes #1 and #2 were 15.1% and 25.9%, respectively. In this case, since the calibration was performed without employing any compensation for Cerenkov radiation, significant signal loss was observed near the ^{192}Ir source position.

DISCUSSION

Signal attenuation through optical fiber

As shown in Fig. 7, Cerenkov signal removal was adequately performed, even if the Cerenkov signals were nine times

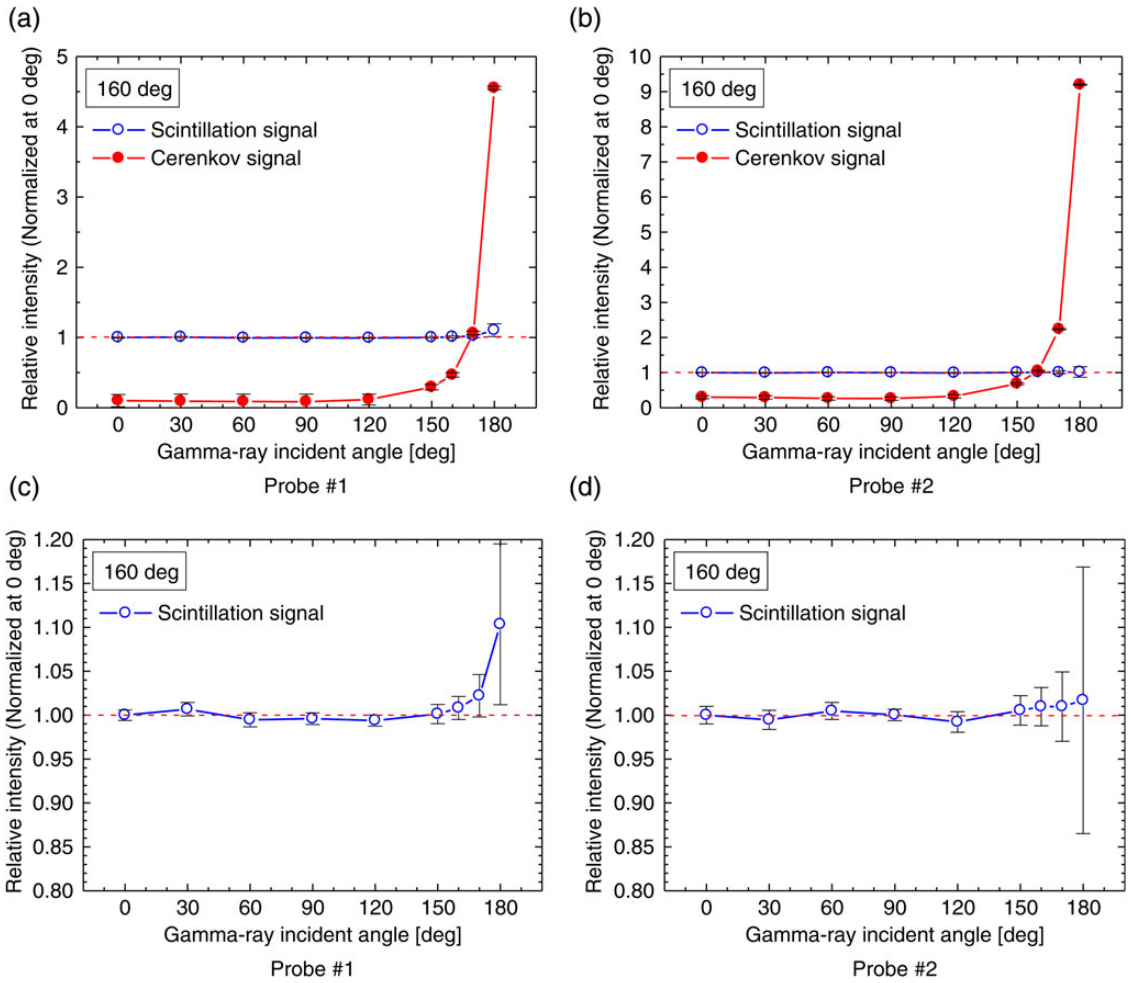

Fig. 6. Separated signals of scintillation and Cerenkov radiation as a function of incident angle for two probes for which calibrations are performed using 0° and 160° source position values. Scintillation and Cerenkov signals (**a, b**) and Scintillation signals fluctuated around a relative intensity of 1.00 (**c, d**).

higher than the scintillation signals. For probe #1, the efficiency fluctuation was less than 1% for all directions; that is, the angular dependency was quite small. The absorbed doses estimated by the two probes were 18.63 ± 0.16 Gy (#1) and 18.58 ± 0.18 Gy (#2) at the measured position in Fig. 5, respectively; measured doses were quite identical.

On the other hand, for the spectrum filtering technique, the possibility exists of efficiency change due to spectrum change that may occur by bending the optical fiber. To confirm the effect of optical fiber bending, wavelength spectra was measured at 180°, as shown in Fig. 5, with the optical fiber lopped five times (diameters 10, 15 and 20 cmϕ) using probe #1 and the USB-2000 spectrometer (manufactured by Ocean Optics Ltd). The relative efficiency for the 10, 15 and 20 cmϕ loops were 1.000 ± 0.0027, 1.005 ± 0.0026 and 1.007 ± 0.0025, respectively. Here, relative efficiency refers to the ratio of the signal value with and without bending of the optical fiber. The efficiency change due to bending an optical fiber seems thus not to be observed. Figure 9 shows the measured wavelength spectra of the scintillation and Cerenkov signals with and without bending using another scintillator-less probe. As shown in Fig. 9, both the scintillation and Cerenkov light spectrum are almost identical, even if the optical fiber was bent with 10 cmϕ × 5 times. For practical usage, looping optical fiber with less than 10 cmϕ diameter is rare; the efficiency due to bending will thus be negligible. The Cerenkov spectrum was different from that reported by Frelin *et al.* (2005) [19], indicating that attenuation of short wavelengths in the optical fiber might occur. However, calibration was performed including such an attenuation effect; influence to the dose evaluation seems therefore to be negligible for light attenuation in the fiber.

Consideration for *in vivo* dosimetry

For ^{192}Ir HDR brachytherapy, the source position frequently changes during treatment, and the Cerenkov signals change

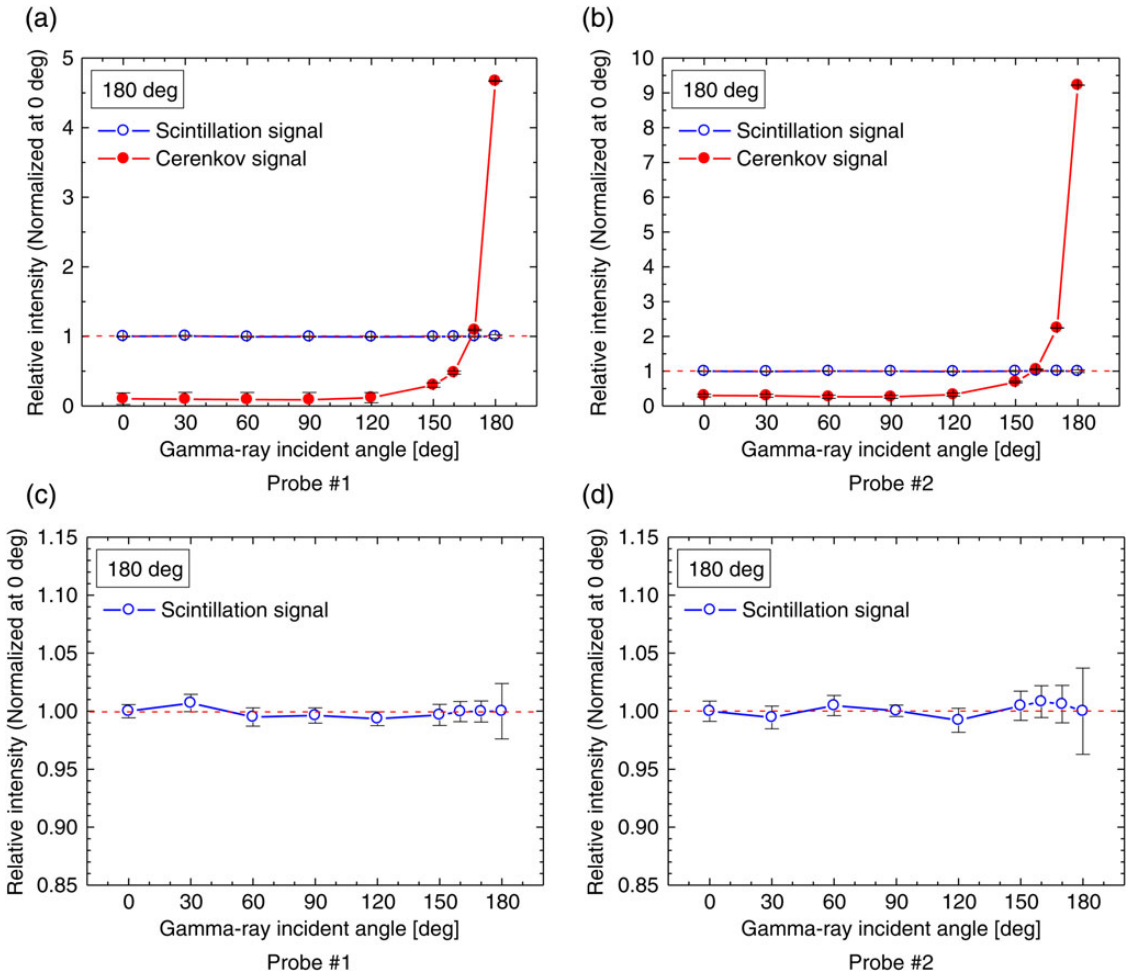

Fig. 7. Separated signals of scintillation and Cerenkov radiation as a function of incident angle for two probes for which calibrations are performed using 0° and 180° source position values. Scintillation and Cerenkov signals (**a, b**) and Scintillation signals fluctuated around a relative intensity of 1.00 (**c, d**).

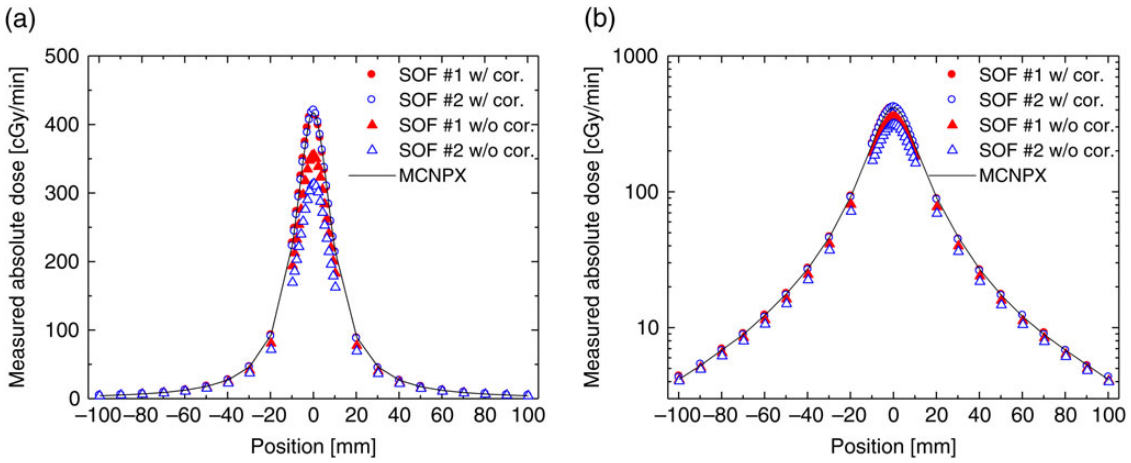

Fig. 8. The result of MCNPX 2.4 calculation and SOF measurement with and without Cerenkov correction. The measured absolute dose in (**a**) linear scale, (**b**) log scale.

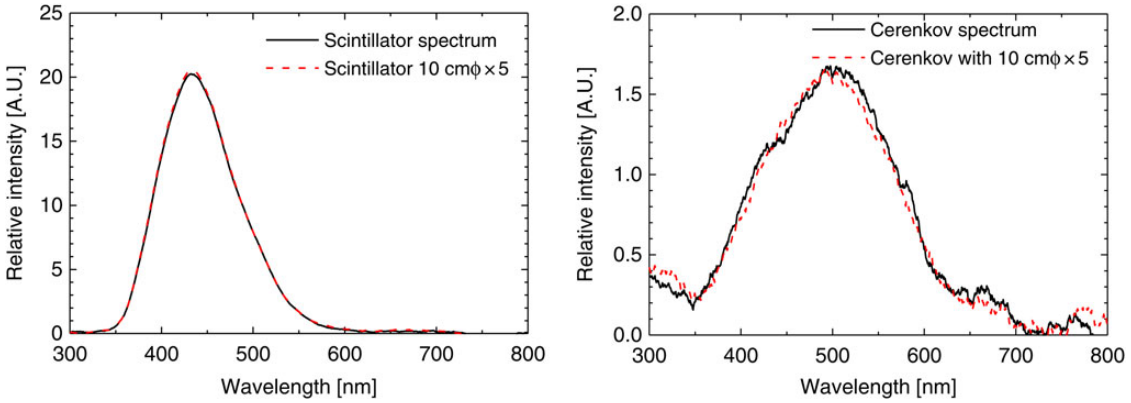

Fig. 9. Spectrum of scintillation and Cerenkov light with and without 10cmϕ × 5 times looped optical fiber.

accordingly. The compensation method should therefore be effective for not only constant conditions but also for such transient situations. Here, the mixture of two situations (Situation A and Situation B), which have the different scintillation signals of S_A and S_B and Cerenkov signals of C_A and C_B, are considered. Note that the count reduction factors a_{Sc} and a_{Cere} are included in each signal in order to simplify the calculation. Signal counts for each channel can be expressed by using Eq. (13) as follows.

$$\begin{pmatrix} Ch1_A & Ch1_B \\ Ch2_A & Ch2_B \end{pmatrix} = \begin{pmatrix} 1 & 1 \\ k_{Sc} & k_{Cere} \end{pmatrix} \begin{pmatrix} S_A & S_B \\ C_A & C_B \end{pmatrix}, \quad (19)$$

where $Ch1_A$ and $Ch1_B$ stand for the signal counts on Ch1 under Situations A and B, respectively, and $Ch2_A$ and $Ch2_B$ stand for signal counts on Ch2 under Situations A and B, respectively. The scintillation signals S_A and S_B are calculated by Eq. (19),

$$S_A = \frac{k_{Cere}Ch1_A - Ch2_A}{k_{Cere} - k_{Sc}} \quad (20)$$

$$S_B = \frac{k_{Cere}Ch1_B - Ch2_B}{k_{Cere} - k_{Sc}}, \quad (21)$$

and the total signal is expressed as

$$S_A + S_B = \frac{k_{Cere}Ch1_A - Ch2_A}{k_{Cere} - k_{Sc}} + \frac{k_{Cere}Ch1_B - Ch2_B}{k_{Cere} - k_{Sc}} = \frac{k_{Cere}(Ch1_A + Ch1_B) - (Ch2_A + Ch2_B)}{k_{Cere} - k_{Sc}}. \quad (22)$$

As shown in Eq. (22), the sum of each scintillation signal is expressed with the sums of each channel. This means that the wavelength-separated SOF dosimeter will be effective in actual measurement, and accurate integral dose can be obtained by using integral counts for each channel.

In practical use, a small-sized probe is better for *in vivo* dosimetry because the dosimeter passes through a small cavity inside the body. The presented dosimeter can compensate for the Cerenkov radiation effect without the reference fiber as necessary in the subtraction method reported previously [10], which facilitates smooth insertion into the patient body. Moreover, since the ^{192}Ir source goes through several catheters, angular dependency is important for accurate *in vivo* dosimetry, and this has been achieved by the hemispherical shape of the scintillator.

CONCLUSIONS

In order to compensate for the Cerenkov radiation effect, input light signals were separated using a dichroic mirror. Signals for high and low wavelengths were counted separately. Measurements with various amounts of Cerenkov radiation were performed by changing the incident direction while keeping the ^{192}Ir source-to-dosimeter distance constant, resulting in a fluctuation of <5%, even if the ^{192}Ir source was placed 2 mm from the optical fiber. Accurate measurement is therefore possible at any source position. For *in vivo* dosimetry, the probe should consist of non-toxic materials and be sterilized. Further investigation will be necessary for applying the proposed dosimeter.

ACKNOWLEDGEMENTS

The authors would like to thank Mao Ohta of the National Hospital Organization Tokyo Medical Center for her assistance.

CONFLICT OF INTEREST

There is no conflict of interest to be disclosed.

FUNDING

This work was partially supported by Grant-in-Aids for Young Scientists (A) (#19689025) by the Ministry of Education, Culture, Sports, Science and Technology.

REFERENCES

1. Quast U, Goncalves J, Schick K *et al*. Multidetector endodosimetry probe with silicon-pn-junction-diodes for in-vivo-dosimetry. *Strahlentherapie* 1979;**155**:489–93.
2. Zilio VO, Joneja OP, Popowski Y *et al*. Absolute depth-dose-rate measurements for an ^{192}Ir HDR brachytherapy source in water using MOSFET detectors. *Med Phys* 2006;**33**:1532–9.
3. Beddar A, Mackie T, Attix F. Cerenkov light generated in optical fibres and other light pipes irradiated by electron beams. *Phys Med Biol* 1992;**37**:925.
4. Beddar A, Mackie T, Attix F. Water-equivalent plastic scintillation detectors for high-energy beam dosimetry: I. Physical characteristics and theoretical considerations. *Phys Med Biol* 1992;**37**:1883.
5. Arnfield MR, Gaballa H, Zwicker R *et al*. Radiation-induced light in optical fibers and plastic scintillators: application to brachytherapy dosimetry. *IEEE Trans Nucl Sci* 1996;**43**: 2077–84.
6. Flühs D, Heintz M, Indenkämpen F *et al*. Direct reading measurement of absorbed dose with plastic scintillators—the general concept and applications to ophthalmic plaque dosimetry. *Med Phys* 1996;**23**:427–34.
7. Geso M, Robinson N, Schumer W *et al*. Use of water-equivalent plastic scintillator for intravascular brachytherapy dosimetry. *Australas Phys Eng Sci Med* 2004;**27**:5–10.
8. Lambert J, McKenzie D, Law S *et al*. A plastic scintillation dosimeter for high dose rate brachytherapy. *Phys Med Biol* 2006;**51**:5505.
9. Sliski A, Soares C, Mitch MG. A fibre optic scintillator dosemeter for absorbed dose measurements of low-energy X-ray-emitting brachytherapy sources. *Radiat Prot Dosimetry* 2006;**120**:24–7.
10. Ishikawa M, Bengua G, Sutherland K *et al*. A feasibility study of novel plastic scintillation dosimetry with pulse-counting mode. *Phys Med Biol* 2009;**54**:2079.
11. Justus BL, Falkenstein P, Huston AL *et al*. Elimination of Cerenkov interference in a fibre-optic-coupled radiation dosemeter. *Radiat Prot Dosimetry* 2006;**120**:20–3.
12. Létourneau D, Pouliot J, Roy R. Miniature scintillating detector for small field radiation therapy. *Med Phys* 1999;**26**:2555–61.
13. Cerenkov PA. Visible glow under exposure of gamma-radiation. *Dokl Akad Nauk SSSR* 1934;**2**:451.
14. Beddar A, Mackie T, Attix F. Water-equivalent plastic scintillation detectors for high-energy beam dosimetry: II. Properties and measurements. *Phys Med Biol* 1992;**37**:1901.
15. Beddar AS, Suchowerska N, Law SH. Plastic scintillation dosimetry for radiation therapy: minimizing capture of Cerenkov radiation noise. *Phys Med Biol* 2004;**49**:783.
16. Clift M, Sutton R, Webb D. Dealing with Cerenkov radiation generated in organic scintillator dosimeters by bremsstrahlung beams. *Phys Med Biol* 2000;**45**:1165.
17. Clift M, Johnston P, Webb D. A temporal method of avoiding the Cerenkov radiation generated in organic scintillator dosimeters by pulsed mega-voltage electron and photon beams. *Phys Med Biol* 2002;**47**:1421.
18. Fontbonne J, Iltis G, Ban G *et al*. Scintillating fiber dosimeter for radiation therapy accelerator. *IEEE Trans Nucl Sci* 2002; **49**:2223–7.
19. Frelin A, Fontbonne J, Ban G *et al*. Spectral discrimination of Čerenkov radiation in scintillating dosimeters. *Med Phys* 2005;**32**:3000–6.
20. Archambault L, Beddar AS, Gingras L *et al*. Measurement accuracy and Cerenkov removal for high performance, high spatial resolution scintillation dosimetry. *Med Phys* 2005;**33**: 128–35.
21. Guillot M, Gingras L, Archambault L *et al*. Spectral method for the correction of the Cerenkov light effect in plastic scintillation detectors: a comparison study of calibration procedures and validation in Cerenkov light-dominated situations. *Med Phys* 2011;**38**:2140–50.
22. Lambert J, Yin Y, McKenzie D *et al*. Cerenkov-free scintillation dosimetry in external beam radiotherapy with an air core light guide. *Phys Med Biol* 2008;**53**:3071.
23. Therriault-Proulx F, Briere TM, Mourtada F *et al*. A phantom study of an *in vivo* dosimetry system using plastic scintillation detectors for real-time verification of 192Ir HDR brachytherapy. *Med Phys* 2011;**38**:2542–51.